

Peculiar characteristics of amplification and noise for intensity modulated light in semiconductor optical amplifier

メタデータ	言語: English 出版者: 公開日: 2017-10-03 キーワード (Ja): キーワード (En): 作成者: Makinoshima-Higuchi, Kazuki, Takeuchi, Nobuhito, Yamada, Minoru メールアドレス: 所属:
URL	http://hdl.handle.net/2297/40177

PAPER

Peculiar Characteristics of Amplification and Noise for Intensity Modulated Light in Semiconductor Optical Amplifier

Kazuki HIGUCHI^{†a)}, Nobuhito TAKEUCHI^{†*}, *Nonmembers*, and Minoru YAMADA^{†b)}, *Member*

SUMMARY Amplification characteristics of the signal and the noise in the semiconductor optical amplifier (SOA), without facet mirrors for the intensity modulated light, are theoretically analyzed and experimentally confirmed. We have found that the amplification factor of the temporarily varying intensity component is smaller than that of the continuous wave (CW) component, but increases up to that of the CW component in the high frequency region in the SOA. These properties are very peculiar in the SOA, which is not shown in conventional electronic devices and semiconductor lasers. Therefore, the relative intensity noise (RIN), which is defined as ratio of the square value of the intensity fluctuation to that of the CW power can be improved by the amplification by the SOA. On the other hand, the signal to the noise ratio (S/N ratio) defined for ratio of the square value of the modulated signal power to that of the intensity fluctuation have both cases of the degradation and the improvement by the amplification depending on combination of the modulation and the noise frequencies. Experimental confirmations of these peculiar characteristics are also demonstrated.

key words: semiconductor optical amplifier, intensity noise, RIN, intensity modulation, S/N ratio

1. Introduction

The semiconductor optical amplifier (SOA) has been in use and its operating mechanism and properties have been investigated by many authors [1]-[18]. Important properties of an amplifier are the amplification factor, the operating power and the noise. In most electronic and optical devices, the amplification factor or the operating range is reduced in the higher frequency region for the modulated signal. Also, the signal to the noise ratio (S/N ratio) or the relative intensity noise (RIN) for the signal is degraded after passing an amplifier, because both the signal and the noise are amplified and additional noise are generated in the amplifier.

However for the SOA which does not have the facet mirrors, several authors have theoretically predicted that the inputted optical signal can reveal the larger amplification factor for the higher modulation frequency than the lower modulation frequency[15], as well as the RIN can be reduced by the amplification[6][7][17]. These peculiar operating characters are opposite to those in conventional electronic amplifiers and semiconductor lasers, but are seemed

not popularly be known yet. One reason of this less popular knowledge may come from the fact that method of theoretical analysis has not been fixed yet, resulting in difficulty to point out clearly the dominant cause or mechanism to generate above mentioned peculiar operating characteristics.

If a SOA consists of two facet mirrors at the input and the output ports, the spontaneous emission can be counted in terms of the longitudinal modes, given with standing waves formed by the two facets mirrors similar as in the semiconductor lasers [1]. For the case of the SOA without facet mirrors, the optical wave is given with propagating traveling wave without boundary condition along the longitudinal direction. Then, almost authors have supposed that sources for the spontaneous emission are spatially localized point sources and should have continuous spectrum. However, the idea of the photon has to be defined together with definition of the mode whose spatial distribution should be well defined with discreet angular frequency in principle.

In the previous paper in Ref.[17], one of current authors proposed a model in which a periodic boundary condition with length L_f is supposed to define longitudinal modes for the spontaneous emission. In the space within length L_f , a single zero-point energy can exist for each longitudinal mode. Then, we can relate L_f with emission rate of the spontaneous emission and count up quantitatively total photon number and amount of the Langevin noise sources giving fluctuations on the photon and the electron numbers.

The RIN is defined as a ratio of auto-correlated value of the fluctuated component to square value of the continuous wave (CW) component of the photon numbers. We have theoretically shown and experimentally confirmed that the RIN becomes reduced after amplification by SOA when the optical power is sufficiently large enough [17][18]. This peculiar property comes from the fact that temporal fluctuation of the electron density has inverse vibrating phase with that of the photon number, resulting in less amplification for the fluctuated photon number. Let us call this effect to be "expulsion effect" here. This expulsion effect does not influence on the CW component which have no temporal variation. Thus the RIN can be improved by the amplification.

Generating question is how is for the intensity modulated light? When the input signal is given with intensity modulated light, the S/N ratio should be defined for ratio of square value of the modulated component to auto-correlated value of the fluctuated component. Because both the modulated and the fluctuated components suffer the expulsion effect, both components must be less amplified.

Manuscript received January 1, 2011.

Manuscript revised January 1, 2011.

[†]The author is with the Division of Electrical Engineering and Computer Science, Graduate School of Natural Science and Technology, Kanazawa University, Kanazawa 920-1192, Japan.

*Presently, the author is with the Hokuriku Electric Power Company Ltd.,Japan.

a) E-mail: me131057@ec.t.kanazawa-u.ac.jp

b) E-mail: myamadaniifty@nifty.com

DOI: 10.1587/transele.E0.C.1

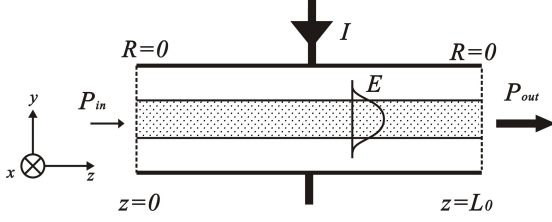


Fig. 1 Structure of semiconductor optical amplifier (SOA). Facets of the amplifier are anti-reflection coated to prevent reflections.

In this paper, we theoretically analyze and experimentally confirm amplification properties of intensity modulated light in the SOA having no facet mirror. Amplifications of the CW, the modulated and the noise components are analyzed and are represented in terms of the RIN and the S/N ratio.

This paper is organized as the followings: In Section II, model and basic equations of this analysis are introduced. In Section III, the optical power and the electron density are decomposed to the CW, modulated and fluctuating components. The model and calculating manner are almost same as in Ref.[17], but the treatment is extended to include the intensity modulation for the imputed light. In Section IV, numerically calculated data are given. In Section V, experimentally measured data are presented and compared with numerically calculated data. In Section VI, conclusions are listed.

2. Model of Theoretical Analysis

Structure of the SOA is illustrated in Fig.1. Inputted light propagates along z direction. Length of the amplifier is L_0 , width and thickness of the active region are w and d , respectively, facets for the input and the output are anti-reflection coated to prevent the reflections. Field distribution in $x - y$ transverse cross-section are supposed to be stable fundamental modes.

In the beginning, we suppose a length L_f in which a longitudinal mode for the traveling wave of the amplified spontaneous emission (ASE) is defined with a periodic boundary condition as

$$\beta_m L_f = \sqrt{\mu_0 \epsilon_0} n_{eq} \omega_m L_f = 2\pi n_{eq} L_f / \lambda_m = 2m\pi, \quad (1)$$

where m is the mode number, β_m is the propagation constant, ω_m is the angular frequency, λ_m is the wavelength and n_{eq} is an equivalent refractive index characterizing the propagation speed v_m of the field as

$$v_m = c/n_{eq}. \quad (2)$$

The photon and photon number S_m are defined in the given space with L_f . Variation of the photon number is derived from the Maxwell's wave equation with suitable quantum mechanical modification as [17]

$$\frac{dS_m(t, z)}{dt} = \frac{\partial S_m}{\partial t} + v_m \frac{\partial S_m}{\partial z}$$

$$= v_m (g_m - \kappa_m) S_m + v_m g_{em} + F_m(t, z), \quad (3)$$

where g_m is the gain coefficient, κ_m is the guiding loss coefficient and $F_m(t, z)$ is the Langevin noise source. Here, the gain coefficient g_m consists of two parts for the optical emission g_{em} and the optical absorption g_{am} , corresponding to the electron transition from the conduction band to the valence band and that from the valence band to the conduction band, respectively.

$$g_m = g_{em} - g_{am}. \quad (4)$$

Since electron transition from the conduction band to the valence band is given with $v_m g_{em} (S_m + 1)$ as summation of the stimulated emission and the spontaneous emission, inclusion of the spontaneous emission is introduced in form of $v_m g_{em}$ in (3).

The carrying optical power $P_m(t, z)$ by propagation is related with the photon number through stored optical energy in the space as

$$S_m \hbar \omega_m = \frac{L_f}{v_m} P_m(t, z). \quad (5)$$

Then, a dynamic equation for the carrying optical power $P_m(t, z)$ is derived from (3) as

$$\begin{aligned} \frac{\partial P_m}{\partial z} + \frac{1}{v_m} \frac{\partial P_m}{\partial t} &= (g_m - \kappa_m) P_m + \frac{\hbar \omega_m v_m g_{em}}{L_f} \\ &+ \frac{\hbar \omega_m}{L_f} F_m(t, z), \end{aligned} \quad (6)$$

Here, we examine the supposed length L_f based on property of the spontaneous emission. The spontaneous emission is generated by existence of the zero-point energy of the optical field, and never duplicated in the defined space at the same time for each longitudinal mode. Time period of the spontaneous emission in a mode is $1/v_m g_{em}$. During this time period, the field propagates the length L_f with velocity v_m . Then we get a relation of

$$L_f = 1/g_{em}. \quad (7)$$

Three dimensional volume V_f in the active region corresponding to the supposed length L_f is

$$V_f = w d L_f = \frac{w d}{g_{em}}. \quad (8)$$

Therefore, variation of the electron density n in the defined volume V_f is given as [17]

$$\frac{dn}{dt} = - \sum_m \frac{g_m P_m}{\hbar \omega_m w d} - \frac{n}{\tau} + \frac{I}{e V_0} + \frac{W(t, z)}{V_f}, \quad (9)$$

where τ is the electron lifetime, e is the elementary charge, $V_0 = w d L_0$ is full volume of the active region in the SOA, $W(t, z)$ is another Langevin noise source for the electron number $n V_f$.

In our analytical model, the SOA is made of InGaAsP system having a quantum well structure in the active region.

Then, gain coefficient g_m shows a saturation phenomenon for the increase in the electron density n . We experimentally examined the gain coefficient in a device and found an approximated function by making best fitting to the experimental data as

$$g_m = \frac{\xi a_m (n - n_g)}{1 + b_m n}, \quad (10)$$

where ξ is a field confinement factor into the active region, n_g is the transparent electron density, a_m and b_m are coefficients characterizing the gain. The term g_{am} for the electron transition from the valence to the conduction bands is given by putting $n = 0$ in (10) as

$$g_{am} = \xi a_m n_g. \quad (11)$$

Here, we should note followings in our model : Although each longitudinal mode of the traveling wave is defined with discrete angular frequency ω_m or wavelength λ_m as given in (1), experimentally measured optical spectrum of the amplified spontaneous emission (ASE) must form continuous profile because each mode show a spectrum broadening caused by temporal variations in both the intensity and the phase. The inputted optical light can be adjusted with one of the longitudinal mode, $m = s$, by suitable selection for locating position of the defined space with L_f . Therefore, orthogonal properties among the inputted optical light ($m = s$) and the ASE modes ($m \neq s$) are thus guaranteed.

3. Amplification for The Intensity Modulated Light

We introduce here intensity modulation of the optical power with frequency $f_M = \Omega_M/2\pi$ for the input signal light of $m = s$ and note modulated components with suffix M . The CW components are indicated with $\bar{}$ and the fluctuated components are expanded with angular frequency Ω . The noise generating terms are expressed as

$$F_m(t, z) = \int F_{m\Omega}(z) e^{j\Omega t} d\Omega, \quad (12)$$

$$W(t, z) = \int W_\Omega(z) e^{j\Omega t} d\Omega. \quad (13)$$

The optical power, the electron density and the gain coefficients are, then, expanded with CW, modulated and fluctuating terms such as

$$\begin{aligned} P_s(t, z) &= \bar{P}_s(z) + \{P_M(z) e^{i\Omega_M t} + c.c.\} + \int P_{s\Omega}(z) e^{j\Omega t} d\Omega \\ &= \bar{P}_s(z) + 2|P_M| \cos(\Omega_M t + \theta_M) + \int P_{s\Omega}(z) e^{j\Omega t} d\Omega \\ &\quad \text{for } m = s, \end{aligned} \quad (14)$$

$$P_m(t, z) = \bar{P}_m(z) + \int P_{m\Omega}(z) e^{j\Omega t} d\Omega \quad \text{for } m \neq s, \quad (15)$$

$$n(t, z) = \bar{n}(z) + \{n_M(z) e^{i\Omega_M t} + c.c.\} + \int n_\Omega(z) e^{j\Omega t} d\Omega, \quad (16)$$

$$\begin{aligned} g_m(t, z) &= \bar{g}_m(z) \\ &+ g'_m \left[\{n_M(z) e^{i\Omega_M t} + c.c.\} + \int n_\Omega(z) e^{j\Omega t} d\Omega \right], \end{aligned} \quad (17)$$

$$\begin{aligned} g_{em}(t, z) &= \bar{g}_{em}(z) \\ &+ g'_{em} \left[\{n_M(z) e^{i\Omega_M t} + c.c.\} + \int n_\Omega(z) e^{j\Omega t} d\Omega \right], \end{aligned} \quad (18)$$

where,

$$g'_m = \frac{d g_m}{d n} = \frac{d g_{em}}{d n} = \frac{\xi a_m (1 + b_m n_g)}{(1 + b_m n)^2}. \quad (19)$$

We should note here that amplitude of the modulated light is $2|P_M(z)|$ and the modulation index M_i is defined as

$$M_i = \frac{2|P_M(z)|}{\bar{P}_s(z)}. \quad (20)$$

Although all other ASE modes ($m \neq s$) have possibility to be modulated through the modulated carrier density n_M , we suppose that this modulation of ASE modes is weak enough.

By substituting above equations to (6) with (7), we get spatial changes of the CW, the modulated and the fluctuating terms as

$$\begin{aligned} \frac{\partial \bar{P}_s}{\partial z} &= (\bar{g}_s - \kappa_s) \bar{P}_s + 2 g'_s \text{Re}(n_M P_M^*) \\ &\quad + v_s \hbar \omega_s (\bar{g}_{es}^2 + 2 g_s'^2 |n_M|^2), \end{aligned} \quad (21)$$

$$\begin{aligned} \frac{\partial \bar{P}_m}{\partial z} &= (\bar{g}_m - \kappa_m) \bar{P}_m + v_m \hbar \omega_m (\bar{g}_{em}^2 + 2 g_m'^2 |n_M|^2) \\ &\quad \text{for } m \neq s, \end{aligned} \quad (22)$$

$$\begin{aligned} \frac{\partial P_M}{\partial z} &= \left(-\frac{j\Omega_M}{v_s} + \bar{g}_s - \kappa_s \right) P_M \\ &\quad + g'_s \left(\bar{P}_s + 2 v_s \hbar \omega_s \bar{g}_{es} \right) n_M, \end{aligned} \quad (23)$$

$$\begin{aligned} \frac{\partial P_{m\Omega}}{\partial z} &= \left(-\frac{j\Omega}{v_m} + \bar{g}_m - \kappa_m \right) P_{m\Omega} \\ &\quad + g'_m \left(\bar{P}_m + 2 v_m \hbar \omega_m \bar{g}_{em} \right) n_\Omega + \hbar \omega_m \bar{g}_{em} F_\Omega, \end{aligned} \quad (24)$$

Similarly by substituting to (9) with (8), we get three equations for the electron density;

$$\frac{I}{e V_o} = \sum_m \frac{\bar{g}_m \bar{P}_m}{\hbar \omega_m w d} + \frac{2 g'_s \text{Re}(n_M P_M^*)}{\hbar \omega_s w d} + \frac{\bar{n}}{\tau}, \quad (25)$$

$$n_M = -\frac{\bar{g}_s P_M}{\{j\Omega_M + \sum_m g'_m \bar{P}_m / \hbar \omega_m w d + 1/\tau\} \hbar \omega_s w d}, \quad (26)$$

$$n_\Omega = \frac{W_\Omega / V_f - \sum_m (\bar{g}_m / \hbar \omega_m w d) P_{m\Omega}}{j\Omega + \sum_m g'_m \bar{P}_m / \hbar \omega_m w d + 1/\tau}. \quad (27)$$

Objectives of our calculation are to follow variations of $\bar{P}_s(z)$, $\bar{P}_m(z)$, $|P_M(z)|^2$ and $\langle P_{m\Omega}^2(z) \rangle$ from (21)–(24) along the propagation in the SOA. Although variations along the propagation will be achieved with numerical integrations, we need more manipulation of equations to be substituted in (21)–(24).

From (26), we get equations of

$$|n_M|^2 = \frac{\bar{g}_s^2 |P_M|^2}{\left\{ \Omega_M^2 + \left(\sum_m g'_m \bar{P}_m / \hbar \omega_m w d + 1/\tau \right)^2 \right\} (\hbar \omega_s w d)^2}, \quad (28)$$

$$\text{Re}(n_M P_M^*) = - \frac{\bar{g}_s |P_M|^2 \left(\sum_m g'_m \bar{P}_m / \hbar \omega_m w d + 1/\tau \right)}{\left\{ \Omega_M^2 + \left(\sum_m g'_m \bar{P}_m / \hbar \omega_m w d + 1/\tau \right)^2 \right\} \hbar \omega_s w d}. \quad (29)$$

By substitution of (26) to (23), we get

$$\frac{\partial P_M}{\partial z} = \left(- \frac{j\Omega_M}{v_s} + \bar{g}_s - \kappa_s - \frac{g'_s \bar{g}_s (\bar{P}_s + 2v_s \hbar \omega_s \bar{g}_{es})}{\left\{ j\Omega_M + \sum_m g'_m \bar{P}_m / \hbar \omega_m w d + 1/\tau \right\} \hbar \omega_s w d} \right) P_M, \quad (30)$$

and

$$\frac{\partial |P_M|^2}{\partial z} = 2 \left[\bar{g}_s - \kappa_s - \frac{g'_s \bar{g}_s (\bar{P}_s + 2v_s \hbar \omega_s \bar{g}_{es}) \left(\sum_m \frac{g'_m \bar{P}_m}{\hbar \omega_m w d} + \frac{1}{\tau} \right)}{\left\{ \Omega_M^2 + \left(\sum_m \frac{g'_m \bar{P}_m}{\hbar \omega_m w d} + \frac{1}{\tau} \right)^2 \right\} \hbar \omega_s w d} \right] |P_M|^2. \quad (31)$$

Similarly by substitution of (27) to (24), we get

$$\begin{aligned} \frac{\partial P_{m\Omega}}{\partial z} &= \left(- \frac{j\Omega}{v_m} + \bar{g}_m - \kappa_m \right) P_{m\Omega} \\ &+ g'_m \left(\bar{P}_m + 2v_m \hbar \omega_m \bar{g}_{em} \right) \frac{\frac{W_\Omega}{V_f} - \sum_p \frac{\bar{g}_p P_{p\Omega}}{\hbar \omega_p w d}}{j\Omega + \sum_p \frac{g'_p \bar{P}_p}{\hbar \omega_p w d} + \frac{1}{\tau}} \\ &+ \hbar \omega_m \bar{g}_{em} F_{m\Omega}. \end{aligned} \quad (32)$$

The terms $F_{m\Omega}$ and W_Ω in (27) and (32) are seeds of the noise called the Langevin noise sources. Although direct determinations of these terms are difficult, we can evaluate whose auto-correlated and cross-correlated values by summing up all dynamics of photons and electrons in (3) and (9) such as [17];

$$\langle F_{m\Omega}^2 \rangle = \frac{\bar{g}_{em} + g_{am} + \kappa_m}{\hbar \omega_m \bar{g}_{em}} \bar{P}_m + v_m \bar{g}_{em}, \quad (33)$$

$$\langle W_\Omega^2 \rangle = \sum_m \frac{\bar{g}_{em} + g_{am}}{\hbar \omega_m \bar{g}_{em}} \bar{P}_m + \frac{\bar{n} V_f}{\tau} + \frac{V_f I}{V_o e}, \quad (34)$$

$$\langle F_{m\Omega} W_\Omega \rangle = \langle W_\Omega F_{m\Omega} \rangle = - \frac{\bar{g}_{em} + g_{am}}{\hbar \omega_m \bar{g}_{em}} \bar{P}_m - v_m \bar{g}_{em}. \quad (35)$$

Since we defined the all longitudinal modes to satisfy the orthogonal relation as given by (1), the Langevin noise sources have no mutual correlations among different modes. Hence, we can suppose that mutual correlations for power fluctuations among different modes are zero, although they might have small correlation through the fluctuation of n_Ω ,

$$\langle P_{m\Omega} P_{p\Omega} \rangle \approx 0 \quad \text{for } p \neq m. \quad (36)$$

Then power fluctuation $\langle P_\Omega^2 \rangle$ for the total modes is given with summed value of the power fluctuation of each mode as

$$\langle P_\Omega^2 \rangle = \left\langle \left(\sum_m P_{m\Omega} \right)^2 \right\rangle = \sum_m \langle P_{m\Omega}^2 \rangle. \quad (37)$$

Although almost theoretical analyses of the SOA by other authors postulate to take into account the so called "beating noise" caused by mutual interactions among the ASE modes and the signal modes, we need not take into account the cross terms among the modes because the orthogonal relations are guaranteed in our model.

To apply these relations in the optical power fluctuation, we reform (32) to following three equations by multiplying $P_{m\Omega}^*$, W_Ω^* and $F_{m\Omega}^*$, respectively:

$$\begin{aligned} \frac{\partial \langle P_{m\Omega}^2 \rangle}{\partial z} &= \left\langle \frac{\partial P_{m\Omega}}{\partial z} P_{m\Omega}^* + P_{m\Omega} \frac{\partial P_{m\Omega}^*}{\partial z} \right\rangle = \\ &2 \left[\bar{g}_m - \kappa_m - \frac{g'_m \bar{g}_m (\bar{P}_m + 2v_m \hbar \omega_m \bar{g}_{em}) \left(\sum_p \frac{g'_p \bar{P}_p}{\hbar \omega_p w d} + \frac{1}{\tau} \right)}{\left\{ \Omega^2 + \left(\sum_p \frac{g'_p \bar{P}_p}{\hbar \omega_p w d} + \frac{1}{\tau} \right)^2 \right\} \hbar \omega_m w d} \right] \langle P_{m\Omega}^2 \rangle \\ &+ \frac{2g'_m (\bar{P}_m + 2v_m \hbar \omega_m \bar{g}_{em})}{V_f} \text{Re} \left\{ \frac{\langle P_{m\Omega} W_\Omega^* \rangle}{-j\Omega + \sum_p \frac{g'_p \bar{P}_p}{\hbar \omega_p w d} + \frac{1}{\tau}} \right\} \\ &+ 2\hbar \omega_m \bar{g}_{em} \text{Re} \langle P_{m\Omega} F_{m\Omega}^* \rangle \end{aligned} \quad (38)$$

$$\begin{aligned} \frac{\partial \langle P_{m\Omega} W_\Omega^* \rangle}{\partial z} &= \left\langle \frac{\partial P_{m\Omega}}{\partial z} W_\Omega^* + P_{m\Omega} \frac{\partial W_\Omega^*}{\partial z} \right\rangle = \\ &\left\{ - \frac{j\Omega}{v_m} + \bar{g}_m - \kappa_m \right\} \langle P_{m\Omega} W_\Omega^* \rangle \\ &- \frac{g'_m \bar{g}_m (\bar{P}_m + 2v_m \hbar \omega_m \bar{g}_{em})}{\left(j\Omega + \sum_p \frac{g'_p \bar{P}_p}{\hbar \omega_p w d} + \frac{1}{\tau} \right) \hbar \omega_m w d} \sum_p \langle P_{p\Omega} W_\Omega^* \rangle \\ &+ \frac{g'_m (\bar{P}_m + 2v_m \hbar \omega_m \bar{g}_{em})}{\left(j\Omega + \sum_p \frac{g'_p \bar{P}_p}{\hbar \omega_p w d} + \frac{1}{\tau} \right) V_f} \langle W_\Omega^2 \rangle \end{aligned}$$

$$+\hbar\omega_m\bar{g}_{em} < F_{m\Omega}W_{\Omega}^* > + \left\langle P_{m\Omega} \frac{\partial W_{\Omega}^*}{\partial z} \right\rangle \quad (39)$$

and

$$\begin{aligned} \frac{\partial < P_{m\Omega}F_{m\Omega}^* >}{\partial z} &= \left\langle \frac{\partial P_{m\Omega}}{\partial z} F_{m\Omega}^* + P_{m\Omega} \frac{\partial F_{m\Omega}^*}{\partial z} \right\rangle \\ &= \left\{ -\frac{j\Omega}{v_m} + \bar{g}_m - \kappa_m - \frac{g'_m \bar{g}_m (\bar{P}_m + 2v_m \hbar\omega_m \bar{g}_{em})}{\left(j\Omega + \sum_p \frac{g'_p \bar{P}_p}{\hbar\omega_p wd} + \frac{1}{\tau} \right) \hbar\omega_m wd} \right\} \\ &\times < P_{p\Omega} F_{m\Omega}^* > + \frac{g'_m (\bar{P}_m + 2v_m \hbar\omega_m \bar{g}_{em})}{\left(j\Omega + \sum_p \frac{g'_p \bar{P}_p}{\hbar\omega_p wd} + \frac{1}{\tau} \right) V_f} < W_{\Omega} F_{m\Omega} > \\ &+ \hbar\omega_m \bar{g}_{em} < F_{m\Omega}^2 > + \left\langle P_{m\Omega} \frac{\partial F_{m\Omega}^*}{\partial z} \right\rangle. \end{aligned} \quad (40)$$

Since calculating the terms $\partial W_{\Omega}^*/\partial z$ and $\partial F_{m\Omega}^*/\partial z$ are difficult, we approximate as follows

$$\begin{aligned} \left\langle P_{m\Omega} \frac{\partial W_{\Omega}^*}{\partial z} \right\rangle &= \left\langle P_{m\Omega}(z) \frac{W_{\Omega}^*(z) - W_{\Omega}^*(z - \Delta z)}{\Delta z} \right\rangle \\ &= \frac{\langle P_{m\Omega}(z) W_{\Omega}^*(z) \rangle}{\Delta z} \left(1 - \frac{\langle P_{m\Omega}(z) W_{\Omega}^*(z - \Delta z) \rangle}{\langle P_{m\Omega}(z) W_{\Omega}^*(z) \rangle} \right) \\ &\simeq \frac{\langle P_{m\Omega}(z) W_{\Omega}^*(z) \rangle}{\Delta z} \left(1 - \sqrt{\frac{\langle W_{\Omega}^2(z - \Delta z) \rangle}{\langle W_{\Omega}^2(z) \rangle}} \right), \end{aligned} \quad (41)$$

$$\begin{aligned} \left\langle P_{m\Omega} \frac{\partial F_{m\Omega}^*}{\partial z} \right\rangle &\simeq \frac{\langle P_{m\Omega}(z) F_{m\Omega}^*(z) \rangle}{\Delta z} \left(1 - \sqrt{\frac{\langle F_{m\Omega}^2(z - \Delta z) \rangle}{\langle F_{m\Omega}^2(z) \rangle}} \right). \end{aligned} \quad (42)$$

We perform numerical integration from $z = 0$ to $z = L_0$, along the propagation for all components of \bar{P}_s , \bar{P}_m , $|P_M|^2$, $\langle P_{m\Omega}^2 \rangle$, $\langle P_{m\Omega} W_{\Omega}^* \rangle$ and $\langle P_{m\Omega} F_{m\Omega}^* \rangle$. Here, we need to pay attention that terms of $\langle P_{m\Omega} W_{\Omega}^* \rangle$ and $\langle P_{m\Omega} F_{m\Omega}^* \rangle$ are given with complex numbers although other terms are given with real numbers.

The initial conditions at $z = 0$ are

$$\bar{P}_s(0) = \bar{P}_{in} \quad \text{for} \quad m = s, \quad (43)$$

$$\bar{P}_m(0) = 0 \quad \text{for} \quad m \neq s, \quad (44)$$

$$|P_M(0)| = \frac{1}{2} (M_i)_{in} \bar{P}_{in} \quad \text{for} \quad m = s, \quad (45)$$

$$\langle P_{s\Omega}^2(0) \rangle = \langle P_{\Omega}^2 \rangle_{in} \quad \text{for} \quad m = s, \quad (46)$$

$$\langle P_{m\Omega}^2(0) \rangle = 0 \quad \text{for} \quad m \neq s, \quad (47)$$

$$< P_{m\Omega}(0) W_{\Omega}^*(0) > = < P_{m\Omega}(0) F_{m\Omega}^*(0) > = 0. \quad (48)$$

Three types of the amplification factor are defined in this paper based on treating components, such as

$$\bar{A}_{signal} \equiv \frac{\bar{P}_{out\ signal}}{\bar{P}_{in}} = \frac{\bar{P}_s(L_0)}{\bar{P}_s(0)} \quad \text{for CW signal mode,} \quad (49)$$

$$\bar{A}_{total} \equiv \frac{\bar{P}_{out\ total}}{\bar{P}_{in}} = \frac{\sum_m \bar{P}_m(L_0)}{\bar{P}_s(0)} \quad \text{for CW total mode,} \quad (50)$$

$$A_M \equiv \left| \frac{P_M(L_0)}{P_M(0)} \right| \quad \text{for modulated component,} \quad (51)$$

Here, suffix *total* means to detect all modes including the ASE modes, and *signal* means to pick up only the signal mode $m = s$ by inserting an optical filter.

The RIN is defined for CW power and the S/N ratio is for the modulated term as

$$RIN_{signal} \equiv \frac{\langle P_{s\Omega}^2 \rangle}{\bar{P}_s^2}, \quad (52)$$

$$RIN_{total} \equiv \frac{\langle P_{\Omega}^2 \rangle}{\bar{P}_{total}^2} = \frac{\sum_m \langle P_{m\Omega}^2 \rangle}{\left(\sum_m \bar{P}_m \right)^2}, \quad (53)$$

$$S/N_{signal} \equiv \frac{2|P_M|^2}{\langle P_{s\Omega}^2 \rangle}, \quad (54)$$

$$S/N_{total} \equiv \frac{2|P_M|^2}{\langle P_{\Omega}^2 \rangle} = \frac{2|P_M|^2}{\sum_m \langle P_{m\Omega}^2 \rangle}. \quad (55)$$

4. Numerical Calculation

The SOA model for numerical calculation is made of In-GaAsP system. We suppose that the half width of the ASE profile is $\Delta\lambda$, the gain coefficients g_m and the spontaneous emissions g_{em} are almost identical within the range of $\Delta\lambda$ such as

$$a_m = a, \quad (56)$$

$$b_m = b, \quad (57)$$

and g_{em} are zero for other modes outside of $\Delta\lambda$.

We put here that number of modes taken into account as the ASE modes is X given by [17]

$$X = 2n_{eq} L_f \Delta\lambda / \lambda^2 - 1 = 2n_{eq} \Delta\lambda / \lambda^2 \bar{g}_e - 1, \quad (58)$$

where two directions of the electric polarization are counted in (58) and one mode is subtracted as the signal mode. Then the terms to count the ASE modes are simply rewritten as

$$\bar{A}_{total} = \frac{\bar{P}_s(L_0) + X \bar{P}_m(L_0)}{\bar{P}_s(0)} \quad \text{where} \quad m \neq s, \quad (59)$$

Table 1 Numerical values of used parameters.

Symbol	Parameter	Value	Unit
w	active region width	2	μm
d	active region thickness	40	nm
L_0	amplifier length	907	mm
V_0	Volume of active region	7.256×10^{-17}	m^3
λ	optical wavelength	1.55	μm
$\hbar \omega$	photon energy	0.8	eV
$\Delta\lambda$	half width of ASE	80	nm
n_g	transparent electron density	2×10^{24}	m^{-3}
τ	electron lifetime	8.6×10^{-10}	s
c/v	equivalent refractive index	3.5	
κ	guiding loss coefficient	3030	m^{-1}
ξ	confinement factor	4.3×10^{-2}	
a	coefficient in the gain	1.345×10^{-19}	m^2
b	coefficient in the gain	3.583×10^{-25}	m^3

$$RIN_{total} = \frac{\langle P_{s\Omega}^2 \rangle + X \langle P_{m\Omega}^2 \rangle}{(\bar{P}_s + X \bar{P}_m)^2} \quad \text{where } m \neq s, \quad (60)$$

$$S/N_{total} = \frac{2 |P_M(z)|^2}{\langle P_{s\Omega}^2 \rangle + X \langle P_{m\Omega}^2 \rangle} \quad \text{where } m \neq s. \quad (61)$$

Used parameters in the numerical calculation are listed in TABLE 1. We numerically determined variations of each value in the SOA along z direction and obtained values at $z = L_0$. Calculated examples of amplification characteristics for modulation frequency f_M are shown in Fig.2, where (a) is for the amplification factors and (b) is the modulation index. Solid lines in (a) indicate the CW components for total modes including the ASE, broken lines indicate the CW components for the signal mode and dotted lines indicate the modulated components. The modulated component is obtained only for the signal mode, because the modulation is given only on the signal mode not other ASE modes. The driving current of $I = 100\text{mA}$ and the modulation index of $(M_i)_{in} = 0.1$ for the input light are suggested. The reason why we suggest the small modulation index M_i is that we are adopting a small signal approximation as defined in (14) without introduction of the nonlinear effects due to large signal amplitude.

As shown in Fig.2(a), the amplification factors for CW components do not vary with f_M , and show slight difference between the total modes and the signal mode when input optical power \bar{P}_{in} is lower than $100\mu\text{W}$ but are almost identical when $\bar{P}_{in} \geq 1\text{mW}$. This situation means that included ASE power is lower than $100\mu\text{W}$.

Figure 2(a) also tells us that modulated components are less amplified than the CW components especially in the lower frequency region, and can approach to the values of the CW components in the higher frequency region. This type of amplification characteristic may be the most unique feature of the traveling wave type optical amplifier never observed in the semiconductor lasers and the electronic amplifiers.

Cause of the reduction of the amplification factor in the low frequency region comes from temporal variation of the electron density n_M . We find a term given as

$g'_s 2v_s \hbar \omega_m \bar{g}_{es} n_M$ in (23) and also find vibrating phase of n_M is inverse to that of P_M as given in (26). Then amplification of P_M is suppressed by the term of $g'_s 2v_s \hbar \omega_m \bar{g}_{es} n_M$ in (23). However, we can not find comparing reduction term in the CW amplification given in (21).

We call this reduction effect to be ‘‘repulsion effect in this paper. This repulsion effect remains in (31) and tells us that releasing condition from this effect is

$$\Omega_M \gg \sum_m \frac{g'_m \bar{P}_m}{\hbar \omega_m w d} + \frac{1}{\tau}. \quad (62)$$

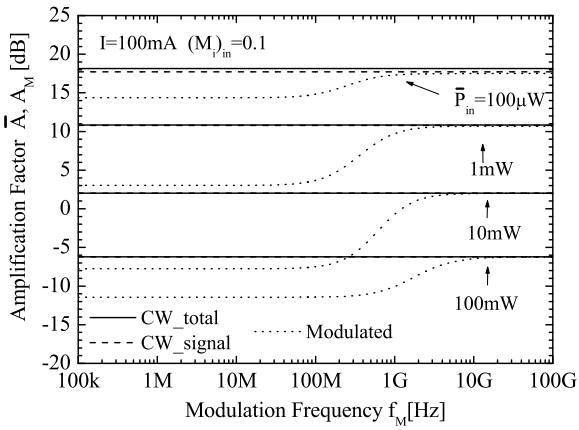
The longer electron lifetime τ and the lower operating power \bar{P}_s are better for the wider frequency range of modulation. This property is completely inverse that of the direct modulation in the semiconductor lasers.

When inputted optical power \bar{P}_m increased from $100\mu\text{W}$ to 10mW , the difference of the amplification factors between CW and Modulated components becomes larger. However, when the input power exceeds 10mW , the difference of the amplification factors between CW and Modulated components becomes smaller. We find from in Fig.2(a) that the CW amplification factor \bar{A} reduces to 0dB around $\bar{P}_m = 10\text{mW}$. It means that the SOA reveals saturation for the amplification for larger input power than 10mW due to reduction of the electron density \bar{n} down to the transparent electron density n_g . Amplification for larger input power such as 100mW , the gain coefficient becomes very small, resulting in smaller difference of the amplification factors between CW and Modulated components.

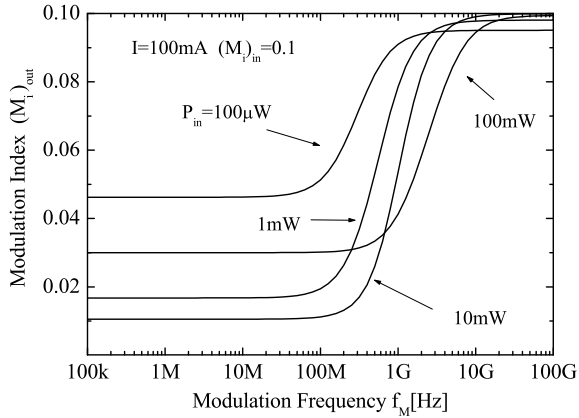
According to the frequency dependence of the amplification factor A_M , the modulation index M_i defined in (20) changes with f_M as shown in Fig.2(b). If the input light is modulated with a pulsation shape in the intensity, the amplified pulse shows different shape from that of the input pulse. However, this type of reformation may not give degradation of the pulse shape, because the higher frequency component is amplified the more effectively than the lower frequency component.

Variations of the amplifications factors with input CW power \bar{P}_{in} are shown in Fig.3, where (a) is for CW components and (b) is for modulated components. Solid lines in (b) are modulation with $f_M = 10\text{GHz}$ and dotted lines are with $f_M = 100\text{MHz}$. Both amplification factors for the CW and modulated components are reduced with increase of the input power because of reduction of the gain \bar{g}_e with the electron density n . If the input optical power \bar{P}_{in} exceeds the supported electrical power of $\hbar \omega_m \times I$, we can not realize the optical amplification any more.

Noise frequency spectrum for the RIN of the output light is given in Fig.4. Horizontal axis is the noise frequency f_N . The RIN level of the input light is assumed to be $RIN_{in} = 1 \times 10^{-14} \text{Hz}^{-1}$ and is indicated with a chain line. The lower RIN is the better for usages. RIN profiles are not changed with the modulation frequency in range of $f_M = 100 \text{kHz}$ to 10GHz . When the driving current I of the SOA and the input optical power \bar{P}_{in} are large enough, RIN of the output light becomes lower than the RIN_{in} in the lower



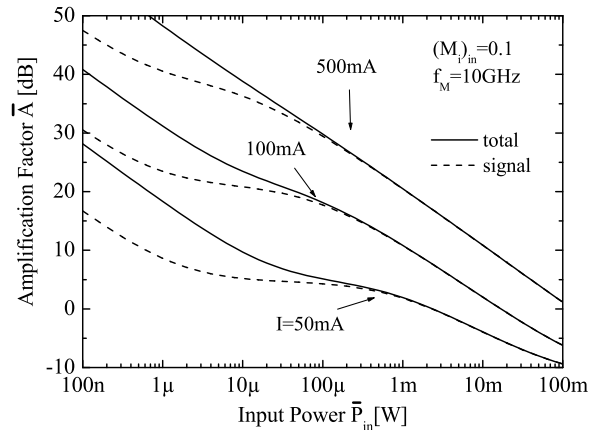
(a) amplification factors



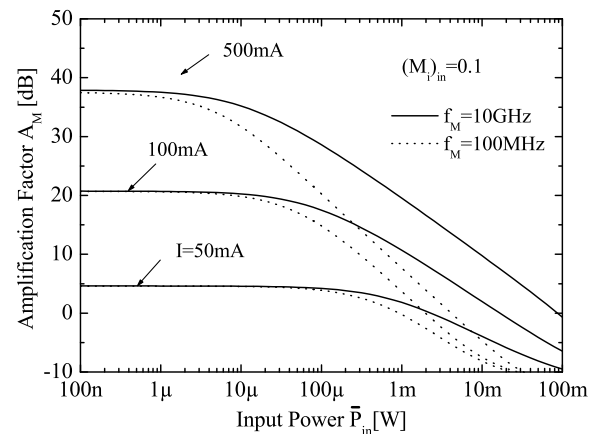
(b) modulation index

Fig. 2 Variations of the amplification factors and modulation index with the modulation frequency.

frequency range than several 100 MHz as already reported in Refs.[17] and [18]. The reason of such improvement of RIN by optical amplification comes from the repulsion effect for noise amplification but not for the CW component as found from (21), (24) and (27). Since both the modulated light and the noise suffer the repulsion effect, the S/N ratio defined in (54) and (55) or (61) reveal rather complicated characteristics. Calculated examples of S/N spectrum are shown in Fig.5 with various frequency f_M of the modulation. The horizontal axis is the noise frequency f_N . The higher S/N ratio is the better for the real usage. The S/N ratio of the input light is indicated with a chain line. The S/N spectrum is sensitively depend on the modulation frequency f_M . When the modulation frequency f_M and the driving current I are large enough, the S/N ratio in the low frequency region becomes higher than that of the input light, resulting in improvement of the S/N ratio by the optical amplification. However, when we measure the noise with same frequency with the modulation frequency $f_M = f_N$, the S/N ratio is



(a) CW components



(b) modulated components

Fig. 3 Variations of the amplification factors with the CW input power.

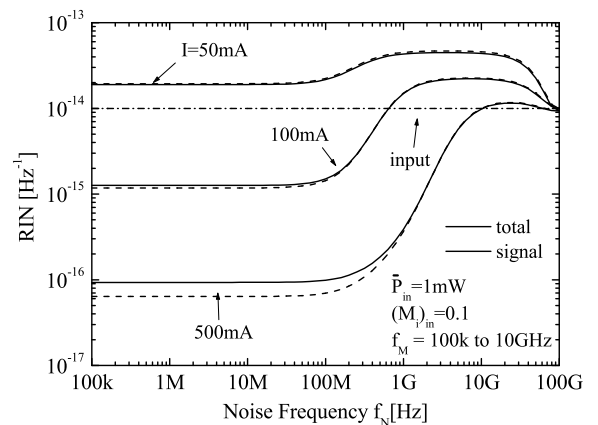
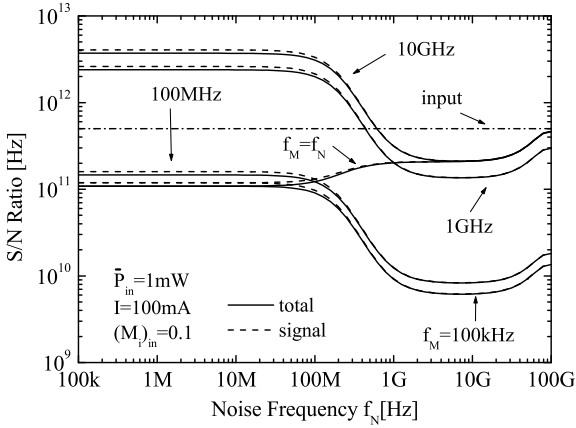
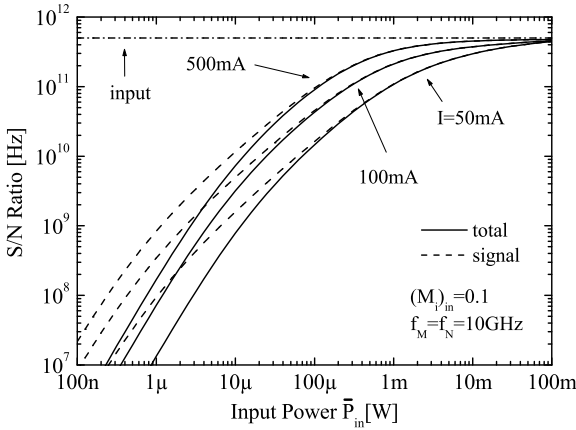


Fig. 4 Frequency spectrum of RIN for intensity modulated light.

degraded by the optical amplification. Variations of the S/N ratio with the input CW optical power \bar{P}_{in} are shown in Fig.6 under condition of $f_M = f_N = 10$ GHz. The S/N ratio of the

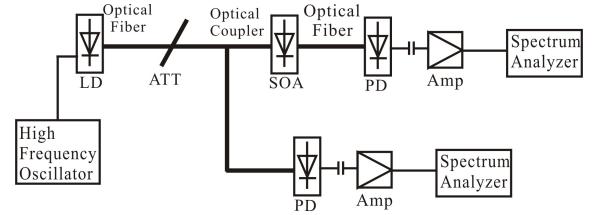
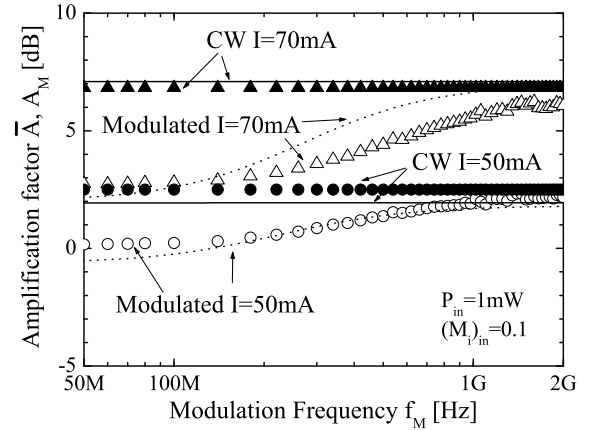

Fig. 5 S/N spectrum.

Fig. 6 Variations of the S/N ratio at $f_N = f_M = 10$ GHz with the CW input power.

input light is indicated with a chain line. The solids lines are S/N ratios when we detect total mode including the ASE modes, and the broken lines are those only for the signal mode which can be picked up by inserting an optical filter. The S/N ratio for the lower input power is much degraded even we use the optical filter.

5. Experimental Confirmation

Setup for the experimental measurements is illustrated in Fig.7. A semiconductor laser (LD) was used as a source of the input light and was modulated with a high frequency oscillator to support intensity modulation on the input light. The RIN level of the input light was fixed by the injection current to the LD, while the input power level to the SOA is adjusted by an optical attenuator (ATT). The CW, the modulated and the noise powers of the input light and the output light from the SOA were evaluated electrically through photo detectors (PD). Oscillation wavelength of the LD was 1545.6nm, modulation index of the inputted optical signal was $(M_i)_{in} = 0.1$. The driving current of the SOA was $I = 50$ mA and $I = 70$ mA.

Relation between the modulation frequency f_M and the


Fig. 7 Configuration of experimental measurements.

Fig. 8 Relation between the modulation frequency f_M and the amplification factor. Solid and dotted lines indicate the theoretical date for CW components \bar{A}_{total} and modulated components A_M . \blacktriangle and \bullet indicate the experimental data for CW components, \triangle and \circ indicate the experimental data for modulated components.

amplification factor is shown in Fig.8. Theoretically calculated data are for the total modes including the ASE modes, because powers of the ASE modes are included in the experiment. The theoretically calculated and the experimentally measured data were well coincided. As seen in Fig.8, amplification factor of the modulated signal is smaller than that of the CW component. In addition, the amplification factor of the modulated light gradually increases with the modulation frequency f_M .

Figure 9 shows relations between the input CW power \bar{P}_{in} and the amplification factors. This figure also indicates good correspondences between the our theoretical analyses and the experiments. Both amplification factors for the CW and modulated components are reduced with increase of the input power, because the electron density in the SOA reduces with increasing of the input power.

On the other hand, when input power is very low such as $\bar{P}_{in} < 100\mu W$, the amplification factors \bar{A} of CW components reveal additionally larger values than the those of the modulated components. This additional enhancement comes from inclusion of the ASE powers, because the ASE powers are included in the CW components but are not in the modulated components.

Relation between the modulation frequency f_M and the RIN at noise frequency $f_N = 100$ MHz is shown in Fig.10. As found from Fig.10, the RIN levels are almost constant for changing of the modulation frequency f_M . When driv-

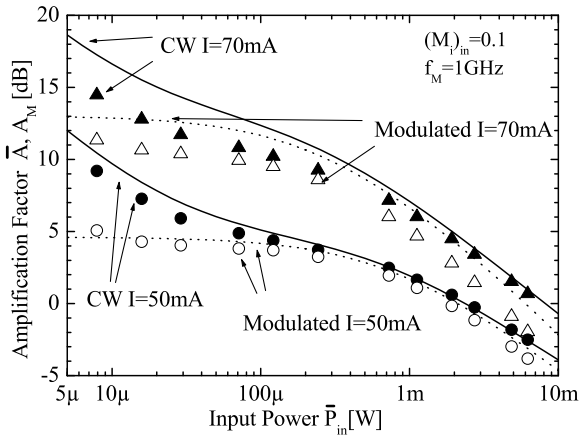


Fig. 9 Relation between the input CW power \bar{P}_{in} and the amplification factor under condition $f_M = 1GHz$. Solid and dotted lines indicate the theoretical date for CW components \bar{A}_{total} and modulated components A_M . \blacktriangle and \bullet indicate the experimental data for CW components, \triangle and \circ indicate the experimental data for modulated components.

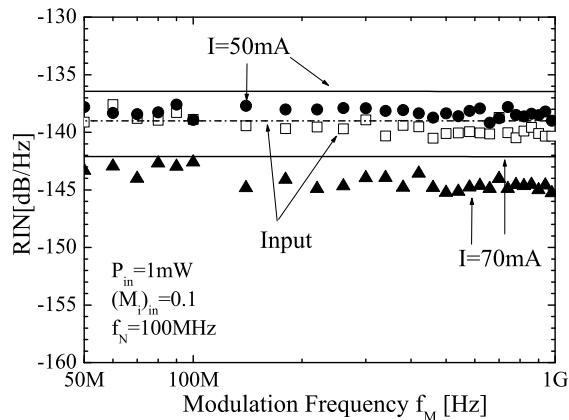


Fig. 10 Relation between the modulation frequency and the RIN at noise frequency $f_N = 100MHz$. Chain lines indicate the theoretical date for RIN of the input light and solid lines correspond to the output light. \square indicate the experimental data for RIN of the input light, and \blacktriangle and \bullet correspond to the output light, respectively.

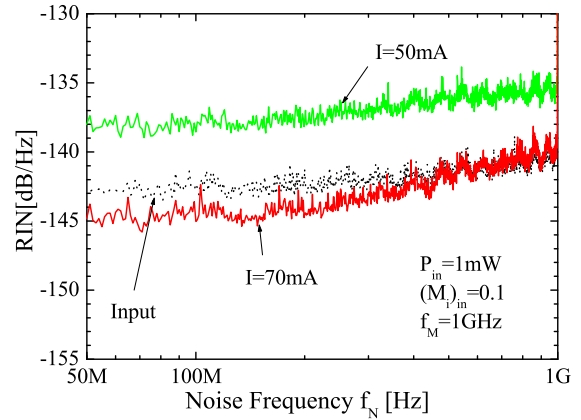
ing current of the SOA is raised up, RIN level of the output is reduced lower than that of the input light, resulting in improvement of the RIN by the optical amplification. This effect means that the repulsion effect affects not on the CW component but on the noise component.

Noise frequency spectrum for the RIN is shown in Fig.11, where (a) is theoretically calculated data, and (b) is experimentally measured data. When the driving current I of the SOA are large enough, RIN of the output light becomes lower than RIN of the input light in the lower frequency region.

Relations between the modulation frequency f_M and the S/N ratio at noise frequency $f_N = 100$ MHz is shown in Fig.12. When modulation frequency is same as the noise frequency $f_M = f_N = 100$ MHz, the S/N ratio of the output light is degraded from that of the input light. However, the S/N ratio of the output is gradually increased with the higher



(a) theoretical results data



(b) experimental results data

Fig. 11 Noise frequency spectrum for the RIN. (a) theoretically calculated data. (b) experimentally measured data.

modulation frequency. The S/N ratio can be improved if the noise is measured with lower frequency than the modulation frequency as $f_M > f_N$.

Figures 13 shows relations between the input CW power \bar{P}_{in} and the S/N ratio at $f_M = f_N = 1GHz$. When we measure the noise with same frequency with the modulation frequency $f_M = f_N$, the S/N ratio is degraded by the optical amplification.

We should note here that the S/N ratio sensitively vary not only with the input optical power, the modulation frequency, the noise frequency and the driving current but also with the modulation index $(M_i)_{in}$. Our theoretical analyses and experimental measurements are performed in the case of small modulation index to investigate basic property of the SOA. If modulation index is large enough, several characteristics may differ from our data as reported in Ref.[14].

As found from these results, our theoretical calculation and postulation were well confirmed by the experimentally obtained data.

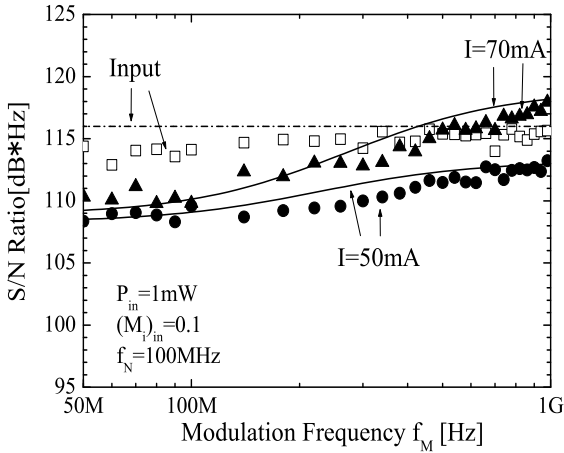


Fig. 12 Relations between the modulation frequency f_M and the S/N ratio at noise frequency $f_N = 100$ MHz. Chain lines indicate the theoretical date for S/N ratio of the input light and solid lines correspond to the output light. \square indicate the experimental data for S/N ratio of the input light, and \blacktriangle and \bullet correspond to the output light, respectively.

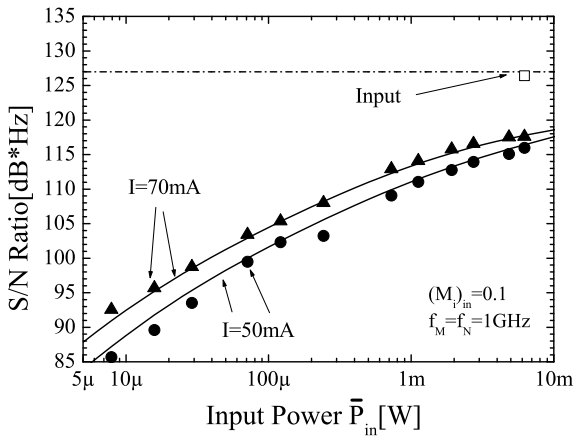


Fig. 13 Relation between the input CW power \bar{P}_m and the S/N ratio under condition $f_M = f_N = 1GHz$. Chain lines indicate the theoretical date for S/N ratio of the input light and solid lines correspond to the output light. \square indicate the experimental data for S/N ratio of the input light, and \blacktriangle and \bullet correspond to the output light, respectively.

6. Conclusion

Characteristics of the amplification and the intensity noise in the SOA (semiconductor optical amplifier) which have no facet mirror for the intensity modulated light are theoretically analyzed and experimentally confirmed. The following peculiar characteristics of the SOA are revealed.

1. Amplification factor of the modulated signal is smaller than that of the CW component. In addition, the amplification ratio of the modulated signal gradually increases with the modulation frequency.
2. The RIN level of the output light is decided by the driving current or output optical power of the SOA. Therefore, RIN can be improved by the optical amplification.

3. The S/N ratio is degraded by the amplification when the noise is measured with almost the same frequency as the modulated signal. However, the S/N can be improved when the modulation frequency of the signal is high enough and the measuring frequency of the noise is low.
4. Above mentioned amplification characteristics are very unique only in the optical amplifier as has not been pointed out in conventional electronic amplifiers and other optical devices such as the semiconductor lasers.

Acknowledgments

The author acknowledge to Dr. H. Shoji, Mr. T. Kaneko and Mr. K. Uesaka of the Sumitomo Electric Industries, Ltd. for cooperative research on this subject. The measured data of the gain coefficient and several parameters in the SOA are obtained by them.

References

- [1] T. Mukai and Y. Yamamoto, "Noise in an AlGaAs semiconductor laser amplifier," *IEEE J. Quantum Electron.*, vol.QE-18, pp.564-575, April 1982.
- [2] T. Saitoh and T. Mukai, "1.5 μ m GaInAsP traveling-wave semiconductor laser amplifier," *IEEE J. Quantum Electron.*, vol.QE-23, pp.1010-1020, June 1987.
- [3] G. P. Agrawal, N. A. Olsson, "Self-modulation and spectral broadening of optical pulses in semiconductor laser amplifier", *IEEE J. Quantum Electron.*, vol.QE-25, pp.2297-2305, November 1989.
- [4] E. Berglind and O. Nilsson, "Laser linewidth broadening caused by a laser amplifier," *IEEE Photon. Technol. Lett.*, vol.3, pp.5, May 1991.
- [5] S. Balsamo, F.Sartori and Montrosset, "Dynamic beam propagation method for flared semiconductor power amplifier," *IEEE J. Selected Topics in Quantum Electron.*, vol.2, pp.378-384, June 1996.
- [6] M. Shtaif and G.Eisenstein, "Noise characteristics of nonlinear semiconductor optical amplifiers in the Gaussian limit," *IEEE J. Quantum Electron.*, vol.32, pp.1801-1809, October 1996.
- [7] M. Shtaif and G.Eisenstein, "Noise properties of nonlinear semiconductor optical amplifiers," *Opt. Letters.*, vol.21, pp.1851-1853, November 1996
- [8] M. J. Munroe, J. Cooper and M. G. Raymer, "Spectral broadening of stochastic light intensity-smoothed by a saturated semiconductor optical amplifier," *IEEE J. Quantum Electron.*, vol.34, pp.548-551, March 1998.
- [9] M.Shtaif, B.Tromborg and G.Eisenstein, "Noise spectra of semiconductor optical amplifiers: Relation between semiclassical and quantum descriptions," *IEEE J. Quantum Electron.*, vol.34, pp.869-877, May 1998.
- [10] A. Champagne, J. Camel, R. Maciejko, K. J. Kasunic D. M. Adams and B. Tromborg, "Linewidth broadening in a distributed feedback laser integrated with a semiconductor optical amplifier," *IEEE J. Quantum Electron.*, vol.38, pp.1493-1502, November 2002.
- [11] G. Morthier, and B. Meyerson, "Intensity noise and line width of laser diodes with integrated semiconductor optical amplifier," *IEEE Photon. Technol. Lett.*, vol.14, pp.1644-1646, December 2002.
- [12] A. Bilenca and G. Eisenstein, "Statistical noise properties of an optical pulse propagating in a nonlinear semiconductor optical amplifier," *IEEE J. Quantum Electron.*, vol.41, pp.36-44, January 2005.
- [13] X. Wei and L. Zhang, "Analysis of the phase noise in saturated SOAs for DPSK applications," *IEEE J. Quantum Electron.*, vol.41, pp.554-561, April 2005.

- [14] T. Briant, P. Grangier, R.T Brouri, A. Bellemain, R. Brenot, and B. Thedrez, "Accurate determination of the noise figure of polarization-dependent optical amplifiers: theory and experiment" *J. of Lightwave Tech.*, vol.24, no.3, pp.1499-1503, March 2006.
- [15] S. Blaaberg and J. Mørk, "General method for calculating the response and noise spectra of active Fabry-Perot semiconductor waveguides with external optical injection," *IEEE J. Quantum Electron.*, vol.45, no.8, pp.950-963, August 2009.
- [16] J. Lloret, F. Ramos, W. Xue, J. Sancho, I. Gassulla, S. Sales, J. Mørk and J. Cpmay, "The influence optical filtering on the noise performance of microwave photonic phase shifters based on SOAs", *J. of Lightwave Tech.*, vol.29, no.12, pp.1746-1752, June 2011
- [17] M. Yamada, "Analysis of intensity and frequency noises in semiconductor optical amplifier," *IEEE J. Quantum Electron.*, vol.48, no.8, pp.980-990, August 2012.
- [18] M. Yamada, N. Takkeuchi, K. Sakumoto, Y. Kuwamura, "Variation of relative intensity noise with optical power in InGaAsP semiconductor optical amplifier" *IEEE Photonic Technology Lett.*, vol.24, No.22, pp.2049-2051, November 2012.



Kazuki Higuchi was born in Niigata, Japan, on September 28, 1990. He received the B.S. degrees in School of Electrical and Computer Engineering from Kanazawa University, Kanazawa, Japan, in 2013. He is currently pursuing the M.S. degree with the Graduate School of Natural Science and Technology, Kanazawa University, Kanazawa, Japan.



Nobuhito Takeuchi was born in Toyama, Japan, on September 12, 1988. He received the B.S. and M.S. degrees in electrical and electronics engineering from Kanazawa University, Kanazawa, Japan, in 2011 and 2013, respectively. He is currently with Hokuriku Electric Power Company, Ltd., Japan.



Minoru Yamada was born in Yamanashi, Japan, on January 26, 1949. He received the B.S. degree in Electrical Engineering from Kanazawa University, Kanazawa, Japan, in 1971, and the M.S. and Ph.D. degrees in Electronics Engineering from Tokyo Institute of Technology, Tokyo, Japan, in 1973 and 1976, respectively. In 1976, he joined Kanazawa University, where he is currently a Professor. From 1982 to 1983, he was a visiting scientist at Bell Laboratories, Holmdel, NJ. His current research

interests include semiconductor lasers and optical amplifiers. Prof. Yamada received the Yonezawa Memorial Prize in 1975, the Paper Award in 1976, and the Achievement Award in 1978 from the Institute of Electronics and Communication Engineers of Japan. He is fellow members of the Japan Society of Applied Physics and IEEE.